Available online at www.sciencedirect.com
SCIENCE DIRECT®
Precision Engineering 29 (2005) 65–80
PRECISION ENGINEERING
www.elsevier.com/locate/precision

Design of integrated eccentric mechanisms and exact constraint fixtures for micron-level repeatability and accuracy

Martin L. Culpepper*, Mangudi Varadarajan Kartik, Christopher DiBiasio

MIT Department of Mechanical Engineering, Room 3-449b, 77 Massachusetts Avenue, Cambridge, MA 02139, USA

Received 21 January 2004; accepted 4 May 2004
Available online 28 October 2004

Abstract

This paper introduces an eccentric ball–shaft kinematic fixture which is capable of six-axis alignment corrections and thereby improved fixture accuracy. A kinematic model for an eccentric ball–shaft fixture was developed and used to simulate the effect of: (1) tolerances, (2) actuation errors and (3) bearing run out on fixture accuracy. The kinematic model and these errors were used to determine when it is practical to use the technology to improve fixture accuracy. The kinematic model was used to design a prototype whose performance matched the kinematic model to within 10%. Diagnosis of experimental data indicates that differences between theory and data may be explained through statistical analysis of error sources. The stabilized 1σ repeatability of the prototype was measured at better than 1.9 μm/3.6 μrad.

Keywords: Accuracy; Precision; Fixture; Pallet; Kinematic coupling; Manufacturing; Exact constraint

1. Introduction

1.1. Fundamental issues of concern for accurate and repeatable fixtures

It is common practice to use a "fleet" of tens to hundreds of fixtures, called pallets, in high-volume manufacturing processes. These pallets transport and align a part to every piece of equipment which processes that part. Given the growing importance of precision manufacturing in high-volume products (e.g. photonics) it has become important to provide palletized fixture systems capable of providing μm/μrad accuracy and repeatability between each pallet and each piece of equipment.

Precision fixtures provide μm/μrad repeatability irrespective of small inaccuracies in their geometry. Fixture accuracy is a kinematic phenomenon and therefore dependant on inaccuracies in the construction and assembly of the fixture. This means that tolerances on contacting elements and contact wear errors will directly affect fixture accuracy. With current manufacturing technology, it is difficult to ensure tolerances better than ±10 μm on placement, ±10 μm on size and ±10 μrad on orientation of each feature on every pallet and the same for the mating features of each piece of equipment. Likewise, the constant engaging and disengaging of fixture contacts makes it difficult to limit the effects of wear on fixture accuracy to less than about 5 μm. Tolerance and wear can easily yield tens of μm/μrad systematic variation (inaccuracy) between fixture pallets as they mate to a given piece of equipment.

As the fixtures must mate to different pieces of equipment, any passive calibration which is set for one machine would not match another machine. Another approach uses a low-precision, palletized system which is augmented with manual alignment or six-axis robotic manipulators and machine vision. This approach is expensive due to the high costs associated with these resources and the need to dedicate resources to each piece of equipment.

In this paper we demonstrate how precision fixture and mechanism technologies may be used to obtain μm/μrad accuracy. We present the theoretical basis for integrated mechanism–fixture technology, a design concept, and a deterministic kinematic modeling approach. Simulated results are

* Corresponding author. Tel.: +1 617 452 2395; fax: +1 509 693 0833.
E-mail address: culpepper@mit.edu (M.L. Culpepper).

0141-6359/$ – see front matter © 2004 Elsevier Inc. All rights reserved.
doi:10.1016/j.precisioneng.2004.05.007

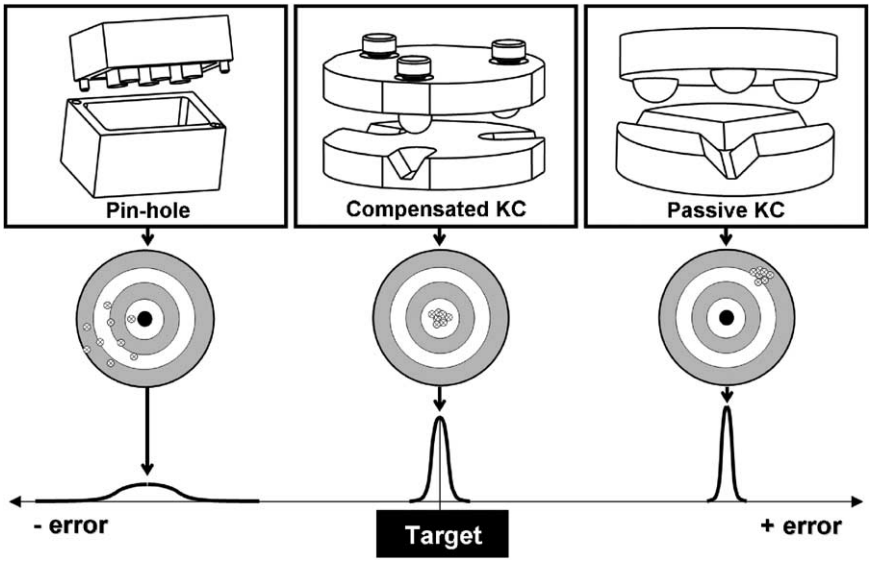

Fig. 1. Accuracy and repeatability of common alignment fixtures.

used to enable designers to ascertain when this technology is a practical alternative to non-mechanized fixture technology. Experimental results are provided to validate the kinematic model and diagnose methods for improving alignment performance.

1.2. Overview of accuracy and repeatability of common fixture types

In Fig. 1, we provide a qualitative comparison of exact constraint (three groove–ball fixtures) and non-exact constraint (pin–slot) fixtures. Fixture wear and manufacturing tolerances lead to inaccuracies in both fixture types, therefore the darts/statistical distribution for each are shifted from the desired target position. Exact constraint fixtures are based upon N independent, near-point contacts which provide μm/μrad repeatability in N degrees of freedom [1]. Exact constraint fixtures limit over constraint and therefore have better repeatability (e.g. less spread).

Most research in precision fixtures has focused on improving the repeatability of exact constraint fixtures [2–6]. Research on accuracy is relatively new, with notable advances in the models which support design decisions [7] and quasi-kinematic couplings [8,9] with sub-micron accuracy and repeatability. The excellent repeatability of exact constraint fixtures makes them a good starting point for providing repeatability and accuracy.

2. Theoretical basis for integrating eccentric mechanisms and exact constraint fixtures

2.1. Previous work in adjustable precision fixtures

It is well known that a three-groove fixture will experience error motions if a ball's center displaces perpendicular to the groove's plane of symmetry (Fig. 2, left) [4]. For instance, an error in the top ball's position will force the other balls to slide in their grooves to maintain geometric compatibility. As a result the coupled components will experience relative movement. On the other hand, this relative motion does not occur when a ball center is displaced along the groove or rotated within the groove (Fig. 2, right). The error motion characteristics of three-groove fixtures has been used to generate concepts which may be extended to correct errors in two [10] and three [11] axes.

2.2. Concepts for six-axis adjustable fixture designs

A precision fixture is kinematically equivalent to a six-axis, parallel mechanism [12]. Fig. 3 helps to illustrate how constraints in a three-groove fixture are equivalent to the constraints (e.g. legs) in a Stewart platform. Six-axis adjustments are therefore possible if the constraining elements (balls and grooves) are moved with respect to the platform to which they are attached. Two examples of adjustable fixture concepts are shown in Fig. 4.

In the left concept, six linear actuators (LA) are used to adjust the position of the six groove surfaces. The six independent actuators are needed to adjust in six axes. In the right concept, a shaft is rigidly attached to each ball with the shaft's axis eccentric ($\boldsymbol{e}$) to the ball center. Three linear-rotary actuators (LRA) act upon the shafts thereby providing six independent actuation inputs. The fixture is in a home (Fig. 5, center) position when the shaft axis lies in the groove's plane of symmetry. When the shafts rotate (Fig. 5, left), the respective shaft axis displaces from the groove's plane of symmetry and planar displacements $\boldsymbol{x}$, $\boldsymbol{y}$ and $\boldsymbol{\theta_z}$ may be obtained. Fig. 6 shows a top view of the fixture in Fig. 5 and the actuation combinations that will produce pure $\boldsymbol{x}$, $\boldsymbol{y}$ or $\boldsymbol{\theta_z}$ displacements. In the figure, the shaft axis is represented as a dot projected on the coupling plane. When the shafts translate along their axes

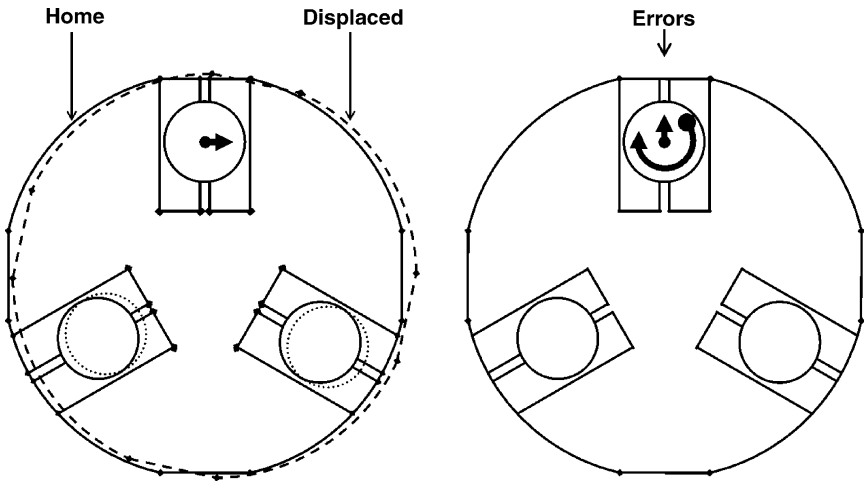

Fig. 2. Error motions generated by ball center displacements and rotations. Left: cross-groove ball displacement generates in-plane coupling displacement. Right: ball displacements along groove generate no coupling displacement.

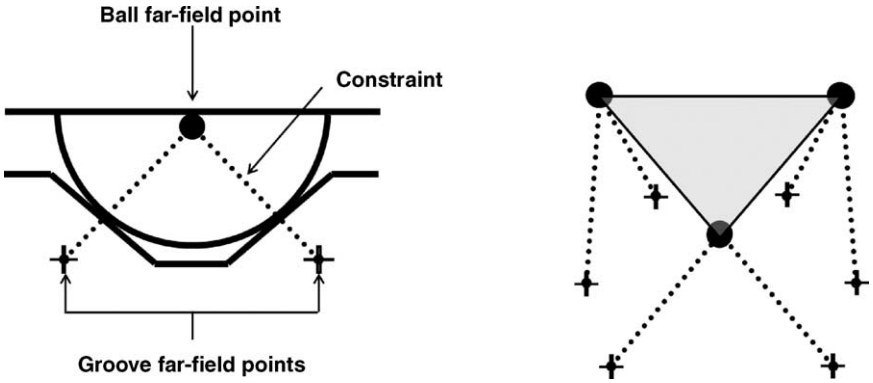

Fig. 3. Analogy between a kinematic fixture and a six-axis parallel mechanism. Left: two constraints at a ball–groove joint. Right: six constraints in a three-groove fixture.

and relative to the top component (Fig. 5, right), non-planar displacement $\boldsymbol{z}$, $\boldsymbol{\theta_x}$ and $\boldsymbol{\theta_y}$ may be obtained.

Work on both fixture concepts is underway, though initial efforts have concentrated on the eccentric ball–shaft design.

3. Kinematic modeling of an eccentric ball–shaft fixture

3.1. In-plane adjustable kinematics

In-plane modeling is based on vector loops through each ball–groove mate. The path of one loop (for ball–groove $\boldsymbol{i} = 1$) is shown in Fig. 7. Fig. 8 shows the projection of the vector loops for each ball–groove set projected on the plane of coupling. The vector loops, share vector $\boldsymbol{r_\Delta} = \boldsymbol{xi} + \boldsymbol{yj}$ between a static centroid attached to the grooved component and a displaced centroid attached to the ball-mounted component.

Two equations (one in $\boldsymbol{x}$ and one in $\boldsymbol{y}$) are extracted from each vector loop and combined to produce the six relationships given in Eq. (1). In this analysis, $\boldsymbol{s}[\theta] = \text{sine}\,[\theta]$ and $\boldsymbol{c}[\theta] = \text{cosine}\,[\theta]$. Subscripts denote variables associated with specific vectors, for instance, $\boldsymbol{\theta_{1a}}$ denotes the direction of vector $\boldsymbol{r_{1a}}$ with respect to the static $\boldsymbol{x}$–$\boldsymbol{y}$ coordinate system. Variables of the form $\boldsymbol{L_{ij}}$ signify the magnitude of vector $\boldsymbol{r_{ij}}$'s projection on the plane of coupling. The length of the eccentricity vector $\boldsymbol{r_{ic}}$ is assigned as a scalar variable, $\boldsymbol{e_i}$.

$$\begin{bmatrix} \boldsymbol{c}[\boldsymbol{\theta_{1a}}] & 0 & 0 & -1 & 0 & L_{1\mathrm{d}} \cdot \boldsymbol{s}[\boldsymbol{\theta_{1a}}] \\ \boldsymbol{s}[\boldsymbol{\theta_{1a}}] & 0 & 0 & 0 & -1 & -L_{1\mathrm{d}} \cdot \boldsymbol{c}[\boldsymbol{\theta_{1a}}] \\ 0 & \boldsymbol{c}[\boldsymbol{\theta_{2a}}] & 0 & -1 & 0 & L_{2\mathrm{d}} \cdot \boldsymbol{s}[\boldsymbol{\theta_{2a}}] \\ 0 & \boldsymbol{s}[\boldsymbol{\theta_{2a}}] & 0 & 0 & -1 & -L_{2\mathrm{d}} \cdot \boldsymbol{c}[\boldsymbol{\theta_{2a}}] \\ 0 & 0 & \boldsymbol{c}[\boldsymbol{\theta_{3a}}] & -1 & 0 & L_{3\mathrm{d}} \cdot \boldsymbol{s}[\boldsymbol{\theta_{3a}}] \\ 0 & 0 & \boldsymbol{s}[\boldsymbol{\theta_{3a}}] & 0 & -1 & -L_{3\mathrm{d}} \cdot \boldsymbol{c}[\boldsymbol{\theta_{3a}}] \end{bmatrix}$$

$$\cdot \begin{pmatrix} L_{1\mathrm{b}} \\ L_{2\mathrm{b}} \\ L_{3\mathrm{b}} \\ \boldsymbol{x} \\ \boldsymbol{y} \\ \boldsymbol{\theta_z} \end{pmatrix} = \begin{pmatrix} e_1 \cdot (\boldsymbol{c}[\boldsymbol{\theta_{1a}}] - \cdot \boldsymbol{c}[\boldsymbol{\theta_{1c}}]) \\ e_1 \cdot (\boldsymbol{s}[\boldsymbol{\theta_{1a}}] - \boldsymbol{s}[\boldsymbol{\theta_{1c}}]) \\ e_2 \cdot (\boldsymbol{c}[\boldsymbol{\theta_{2a}}] - \cdot \boldsymbol{c}[\boldsymbol{\theta_{2c}}]) \\ e_2 \cdot (\boldsymbol{s}[\boldsymbol{\theta_{2a}}] - \boldsymbol{s}[\boldsymbol{\theta_{2c}}]) \\ e_3 \cdot (\boldsymbol{c}[\boldsymbol{\theta_{3a}}] - \cdot \boldsymbol{c}[\boldsymbol{\theta_{3c}}]) \\ e_3 \cdot (\boldsymbol{s}[\boldsymbol{\theta_{3a}}] - \boldsymbol{s}[\boldsymbol{\theta_{3c}}]) \end{pmatrix} \quad (1)$$

When all vectors $\boldsymbol{r_{ic}}$ are aligned with their respective groove's plane of symmetry, e.g. $\boldsymbol{\theta_{ic}} = \boldsymbol{\theta_{ia}}$, the fixture lies in its home

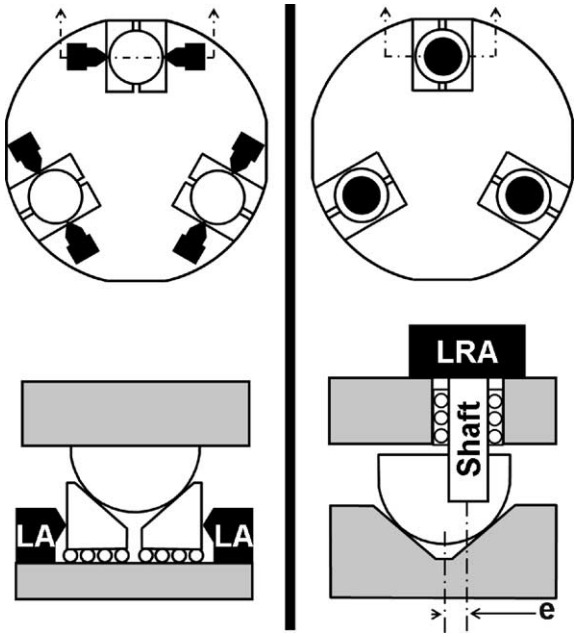

Fig. 4. Concepts for achieving adjustability. Left: linear groove design. Right: eccentric ball–shaft design. *Note:* LA, linear actuator; and LRA, linear-rotary actuator.

Table 1
Scaling of fixture error range (standard deviation) with fixture geometry

Variable	Scales linearly with
$\boldsymbol{r}$	e, σ, RO
$\boldsymbol{z}$	σ
$\boldsymbol{\theta_z}$	$(R/e)^{-1}$, σ, RO
$\boldsymbol{\theta_p}$	R^{-1}, σ

e: Eccentricity, R: coupling radius, σ: standard deviation, RO: run out.

3.2. Out-of-plane adjustable kinematics

Out-of-plane position changes occur with respect to a homed position where the:

- Balls centers are located the same distance from the component their shafts are housed within.
- Opposing faces of the aligned components are parallel.

A plane containing the centers of the balls is defined in this position. Out-of-plane displacements are captured using the translations of the eccentric ball–shaft sets with respect to the top platform. The home and displaced planes are illustrated in Fig. 9. Given the equation of each plane, we then find the difference between the out-of-plane positions of each plane using Eqs. (2)–(4).

$$\boldsymbol{\theta_x} \approx -\frac{L_{1d}\cdot(\boldsymbol{s}[\boldsymbol{\theta_{1a}}]\cdot\theta_z-\boldsymbol{c}[\boldsymbol{\theta_{1a}}])\cdot(z_2-z_3)+L_{2d}\cdot(\boldsymbol{s}[\boldsymbol{\theta_{2a}}]\cdot\theta_z-\boldsymbol{c}[\boldsymbol{\theta_{2a}}])\cdot(z_3-z_1)+L_{3d}\cdot(\boldsymbol{s}[\boldsymbol{\theta_{3a}}]\cdot\theta_z-\boldsymbol{c}[\boldsymbol{\theta_{3a}}])\cdot(z_1-z_2)}{L_{1d}\cdot L_{2d}\cdot\boldsymbol{s}[\boldsymbol{\theta_{2a}}-\boldsymbol{\theta_{1a}}]+L_{2d}\cdot L_{3d}\cdot\boldsymbol{s}[\boldsymbol{\theta_{3a}}-\boldsymbol{\theta_{2a}}]+L_{3d}\cdot L_{1d}\cdot\boldsymbol{s}[\boldsymbol{\theta_{1a}}-\boldsymbol{\theta_{3a}}]} \tag{2}$$

$$\boldsymbol{\theta_y} \approx \frac{L_{1d}\cdot(\boldsymbol{s}[\boldsymbol{\theta_{1a}}]+\boldsymbol{c}[\boldsymbol{\theta_{1a}}]\cdot\theta_z)\cdot(z_2-z_3)+L_{2d}\cdot(\boldsymbol{s}[\boldsymbol{\theta_{2a}}]+\boldsymbol{c}[\boldsymbol{\theta_{2a}}]\cdot\theta_z)\cdot(z_3-z_1)+L_{3d}\cdot(\boldsymbol{s}[\boldsymbol{\theta_{3a}}]+\boldsymbol{c}[\boldsymbol{\theta_{3a}}]\cdot\theta_z)\cdot(z_1-z_2)}{L_{1d}\cdot L_{2d}\cdot\boldsymbol{s}[\boldsymbol{\theta_{2a}}-\boldsymbol{\theta_{1a}}]+L_{2d}\cdot L_{3d}\cdot\boldsymbol{s}[\boldsymbol{\theta_{3a}}-\boldsymbol{\theta_{2a}}]+L_{3d}\cdot L_{1d}\cdot\boldsymbol{s}[\boldsymbol{\theta_{1a}}-\boldsymbol{\theta_{3a}}]} \tag{3}$$

$$\boldsymbol{z_c} \approx L_{1d}\cdot(\boldsymbol{\theta_y}\cdot\boldsymbol{c}[\boldsymbol{\theta_{1a}}]-\boldsymbol{\theta_x}\cdot\boldsymbol{s}[\boldsymbol{\theta_{1a}}])+z_1 \tag{4}$$

In Eqs. (2)–(4), $\boldsymbol{z_i}$ denotes the displacement of the center of ball $\boldsymbol{i}$ from its home position.

position and the static and displaced coordinate systems $\boldsymbol{x}$–$\boldsymbol{y}$ and $\boldsymbol{x}'$–$\boldsymbol{y}'$ are coincident. Vectors $\boldsymbol{r_{ia}}$ and $\boldsymbol{r_{ib}}$ lie along the plane of symmetry of groove $\boldsymbol{ia}$. In developing this set of equations we have assumed small angle rotations (less than 1000 μrad) about the $\boldsymbol{z}$-axis and therefore have linearized $\boldsymbol{\theta_z}$. Given the fixture geometry, Eq. (1) can be solved for $\boldsymbol{x}$, $\boldsymbol{y}$ and $\boldsymbol{\theta_z}$ displacements.

3.3. Implementation of kinematic theory in a spreadsheet model

The theory was incorporated into an Excel spreadsheet (available for download at psdam.mit.edu/tools/index.html) which solves forward and reverse kinematics for the

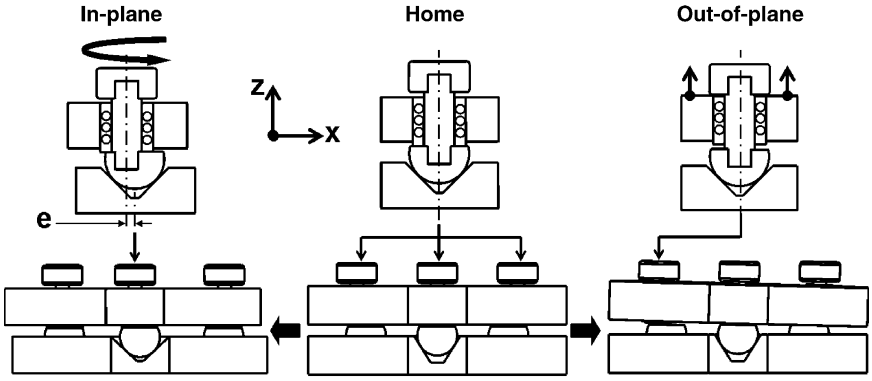

Fig. 5. Generating in-plane (left) and out-of-plane (right) displacements with an eccentric ball–shaft concept. Center shows home position.

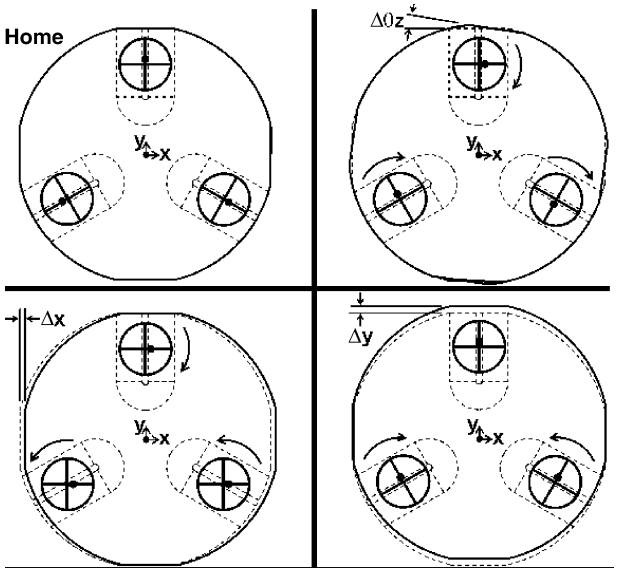

Fig. 6. Schematics showing examples of in-plane displacement generation.

fixture. The accuracy of the kinematic model was checked by comparing predicted displacements with displacements measured from a solid model of an eccentric ball–groove fixture. The difference between predicted and measured results was less than 10 nm/5 μrad, over the eccentric range (range = eccentricity = 125 μm) in each of the following scenarios:

(1) The planar displacement $\boldsymbol{x}$, $\boldsymbol{y}$ and $\boldsymbol{\theta_z}$ examples portrayed in Fig. 6.
(2) The non-planar displacements, $\boldsymbol{\theta_x}$, $\boldsymbol{\theta_y}$ and $\boldsymbol{z}$.
(3) Various combinations of planar and non-planar displacements.

The spreadsheet is equipped to assign fixture geometry parameters as random variables and measure the effect on fixture accuracy. Simulated results show that systematic and non-systematic errors scale linearly with the fixture characteristics in Table 1. The plots in the following sub-sections can be used with these scaling rules to generalize statistical analyses to other eccentric ball–shaft fixture designs. We will assess the statistical nature of fixture performance by examining two planar displacements ($\boldsymbol{r} = \boldsymbol{xi} + \boldsymbol{yj}$ and $\boldsymbol{\theta_z}$) and two non-planar displacements ($\boldsymbol{z}$ and $\boldsymbol{\theta_r} = \boldsymbol{\theta_{xi}} + \boldsymbol{\theta_{yj}}$).

3.4. Systematic errors due to machining and assembly tolerances

We must know the magnitude of a fixture's inaccuracy before we: (a) justify the use of a mechanism–fixture and (b) set the range of a mechanism–fixture. This information was obtained from a simulation in which actuation errors and run out errors were not considered. The results provided in Fig. 10 shows how 6σ machining tolerance of 10 μm and 6σ assembly tolerance of 10 μm affect fixture accuracy. Due to the absence of actuation and run out errors, these results may be applied to: (1) a passive three-groove fixture and (2) an eccentric ball–shaft fixture.

3.5. Random errors due to bearing run out

In this analysis bearing-shaft run out was the only source of error within the fixture. Fig. 11 can be used with the scaling laws in Table 1 to determine how the standard deviation of in-plane errors scale with bearing-shaft run out.

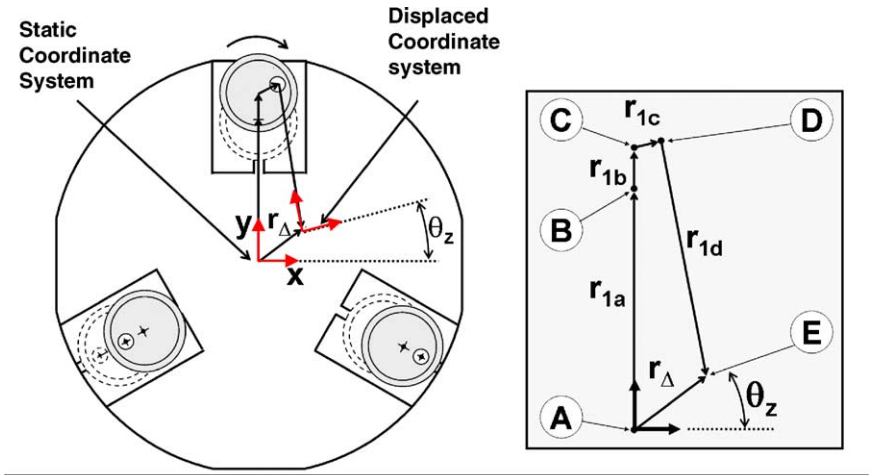

Legend for ball-groove 1 kinematic chain			
A.	Centroid: Grooved component	C.	Ball center displaced from home
B.	Ball center at home position	D.	Shaft axis
E.	Centroid: ball-mounted component		

Fig. 7. Kinematic chain through one ball–groove joint.

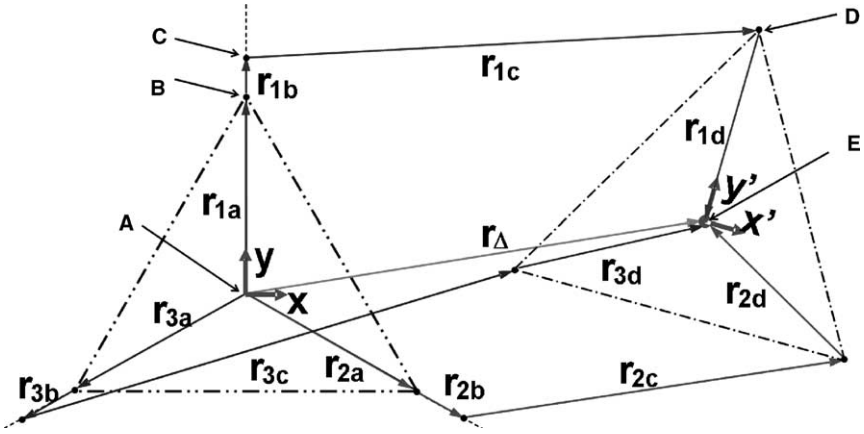

Fig. 8. Vector-based kinematic model for in-plane displacements.

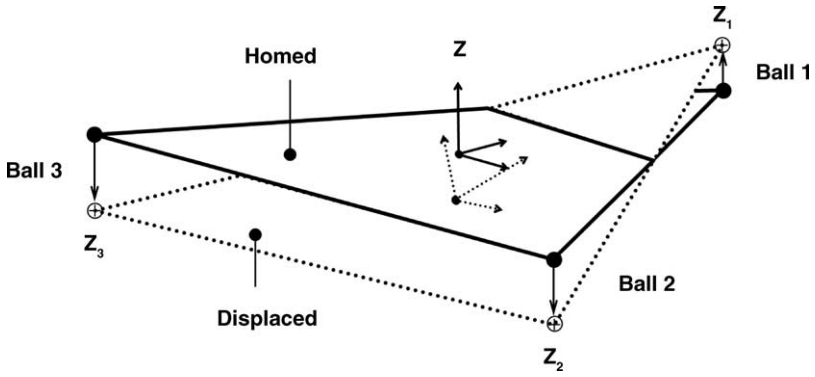

Fig. 9. Homed and displaced planes used in non-planar kinematic modeling.

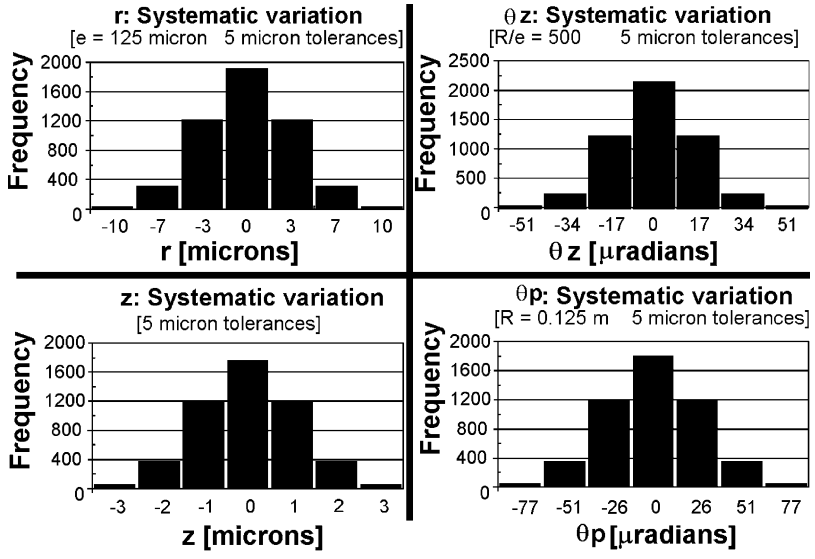

Fig. 10. Effect of manufacturing and assembly tolerances on planar ($\boldsymbol{r}$ and $\boldsymbol{\theta_z}$) and non-planar ($\boldsymbol{z}$ and $\boldsymbol{\theta_p}$) accuracy.

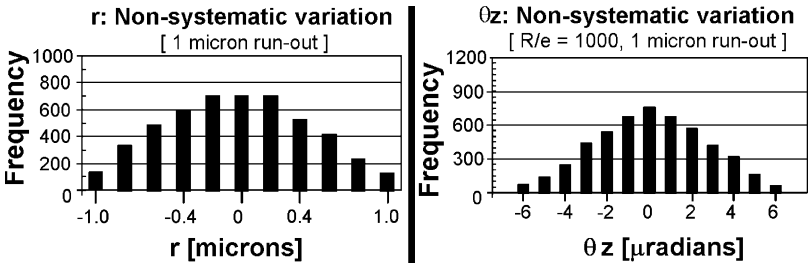

Fig. 11. Effect of bearing-shaft run out on in-plane displacements.

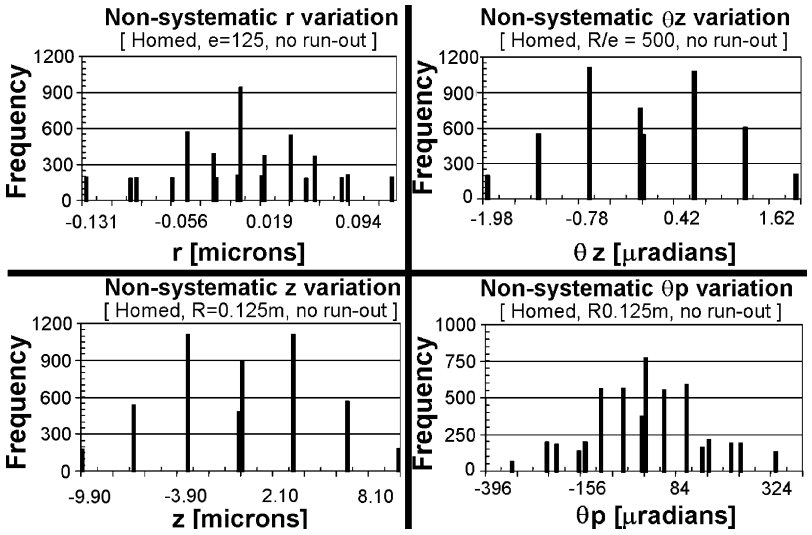

Fig. 12. Effect of digital actuation errors on planar ($\boldsymbol{r}$ and $\boldsymbol{\theta_z}$) and non-planar ($\boldsymbol{z}$ and $\boldsymbol{\theta_p}$) accuracy.

3.6. Random errors due to actuation inputs

Two-axis actuators contain stepper motors which can be modeled as having an equal probability of positioning at either $-s$, 0, or $+s$. Here s is the step size of the motor. In this simulation, values of $s_{\text{rotation}} = 0.054^\circ$ and $s_{\text{translation}} = 5\,\mu\text{m}$ were used. The digital nature of the results in Fig. 12 reflects the digital nature of the actuator errors. Again, the spread in errors scale according to the rules provided in Table 1.

3.7. Comparing manufacturing/assembly errors with mechanism errors

The decision to use mechanism–fixture technology over passive fixture technology depends on the performance benefit that can be realized. The decision process would need to consider the inaccuracy due to fixture manufacturing and assembly (IA_{mfg}) as well as inaccuracy from the mechanism (IA_{mec}). As the ratio of $\text{IA}_{\text{mfg}}/\text{IA}_{\text{mec}}$, increases beyond unity,

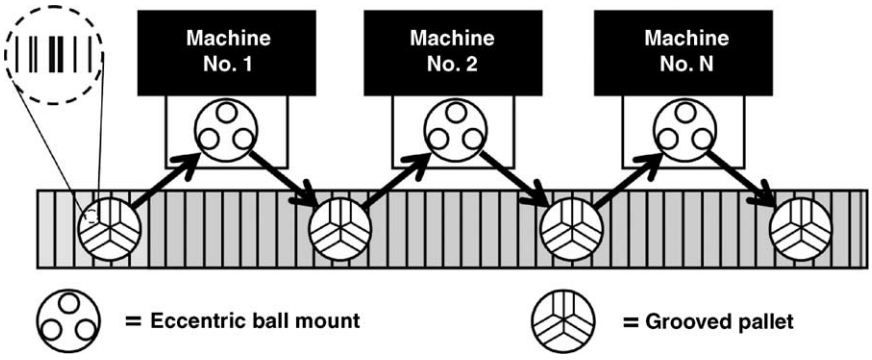

Fig. 13. Precision machining process with precision, palletized kinematic fixtures.

more performance benefit may be gained for a given design. The models and statistical analyses can be coupled with cost analyses to generate a cost–performance relationship for both fixture technologies. Engineers and managers can use this information to find break points and make early design decisions.

4. Design of an eccentric ball–shaft fixture

4.1. Use of mechanism–fixture concept in a palletized fixture systems

An illustration of an example process using mechanism–fixture technology is provided in Fig. 13. Grooved pallets are marked with a passive identifier (bar code or RFID tag) which characterizes the pallet's systematic error set (SES). Each machining station is equipped with three actuated ball–shaft sets and information regarding the SES associated with the same. Using the theory provided in Section 3, the pallet's SES and the machine's SES; each station may then actuate its ball–shaft sets to obtain an accurate and repeatable mate to each pallet.

4.2. Main components and characteristics of the prototype

A prototype fixture was designed using the theory and modeling tools discussed in Section 3. Fig. 14 shows the components of the prototype. The eccentric ball–shaft sets are actuated by three linear-rotary actuators capable of simultaneous shaft rotation (0.056 degree resolution) and translation (0.4 μm resolution). The ball and groove surfaces were polished to 90 nm roughness and coated with TiN coating to minimize wear-in errors and reduce wear of the contacting surfaces [13]. The ball eccentricities were set at significantly different values to show that the kinematic theory could be used to take differences in eccentricity into account when predicting fixture motion. Approximately 20% of the difference between the eccentricity values is due to manufacturing and assembly error. Other characteristics of the fixture are listed in Table 2.

Table 2
Characteristics of prototype fixture

Coupling diameter	152.4 mm
Ball primary radii of curvature	63.5 and 31.75 mm
Ball 1 eccentricity	165 μm
Ball 2 eccentricity	318 μm
Ball 3 eccentricity	363 μm
Ball–groove material	304L stainless
Included groove angle	90°
Surface treatment	Balls grooves protected by a 3.5 μm TiN coating (HRC 88)

4.3. Design to minimize errors from actuators and bearings

The major components of the fixture are detailed in the exploded view of Fig. 15 and the section view of Fig. 16. The wobble and run out of shafts are potential sources of non-systematic errors. These error sources were mitigated using the following design strategies:

4.4. Eccentric ball–shaft bearing errors

Clearance between the shaft and bearings was not acceptable, therefore matched shaft-bearing sets with 5 μm diametral interference were used. These bearings are designed to permit shaft translation and rotation. Through testing, we have found that the interference fit increases the rolling friction somewhat, but does not affect the actuator's ability to increment at its specified step sizes. These tests have not produced a bearing failure to date. The run out of the bearing-shaft sets was measured at 1.5 μm.

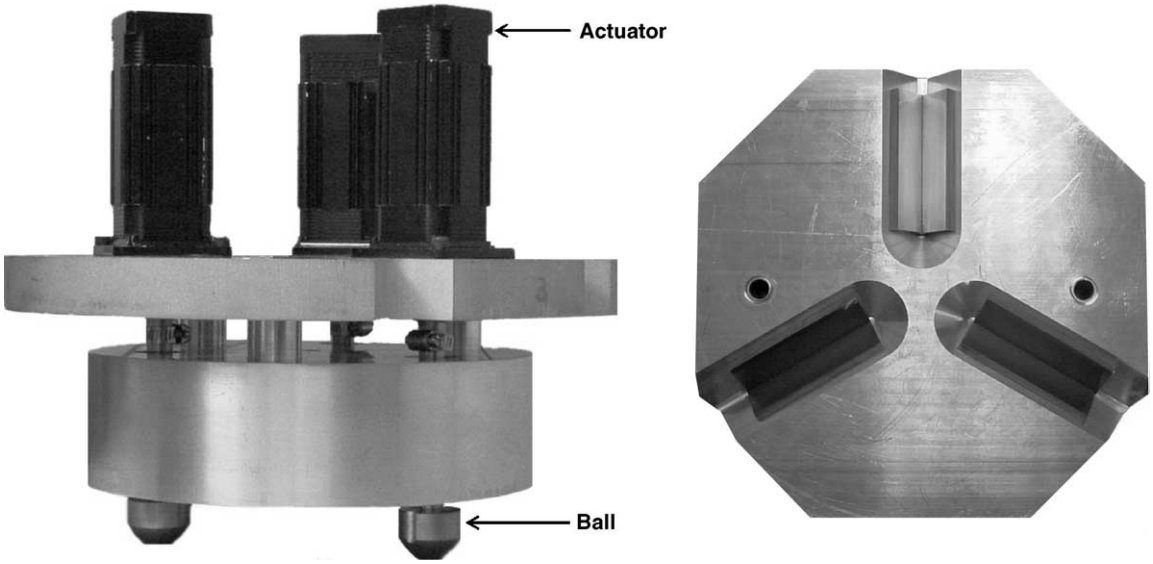

Fig. 14. Major sub-assemblies of eccentric ball–shaft prototype. Left: eccentric balls with linear-rotary actuators. Right: grooved pallet.

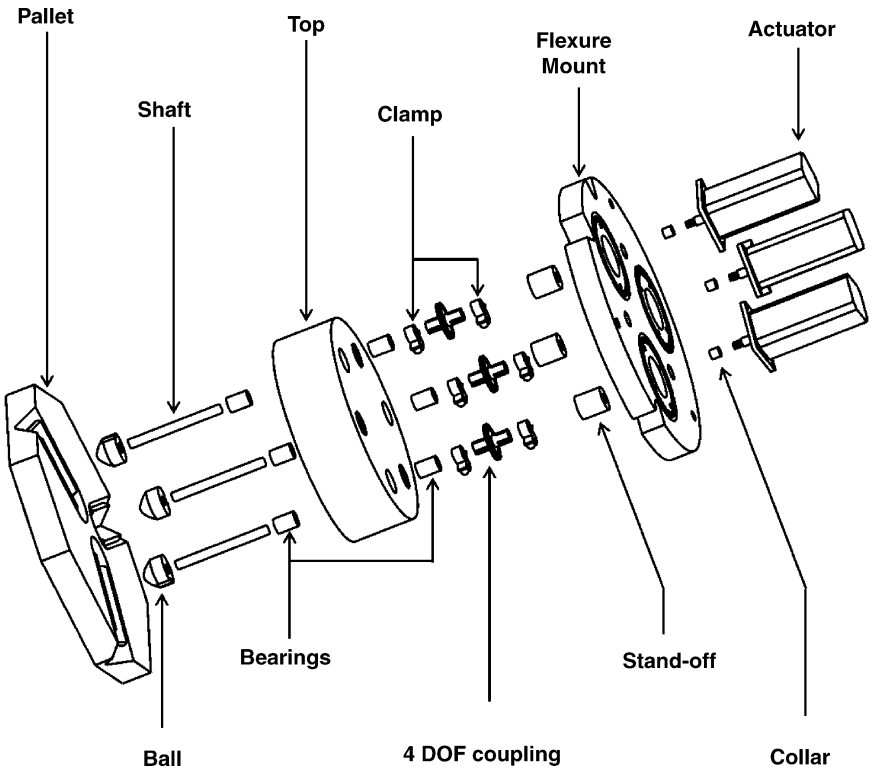

Fig. 15. Exploded view of eccentric ball–shaft fixture prototype.

4.5. Actuator shaft coupling

Three, four DOF flexure couplings filtered the run out and non-perpendicularity errors between the actuator shaft and the eccentric ball–shaft assembly. The couplings, shown in Fig. 17 are designed to be stiff along the shaft axis, stiff in rotation about that axis and compliant in all other (non-actuated) directions.

4.6. Flexure mount for actuators

The monolithic flexure mount contains three four DOF flexures which constrain the actuators in the direction of their actuation. These flexure mounts are shown in Fig. 18. This is essentially a duplication of the function of the four DOF coupling, but provides additional actuator error filtering (increased compliance) which could not be extracted from more

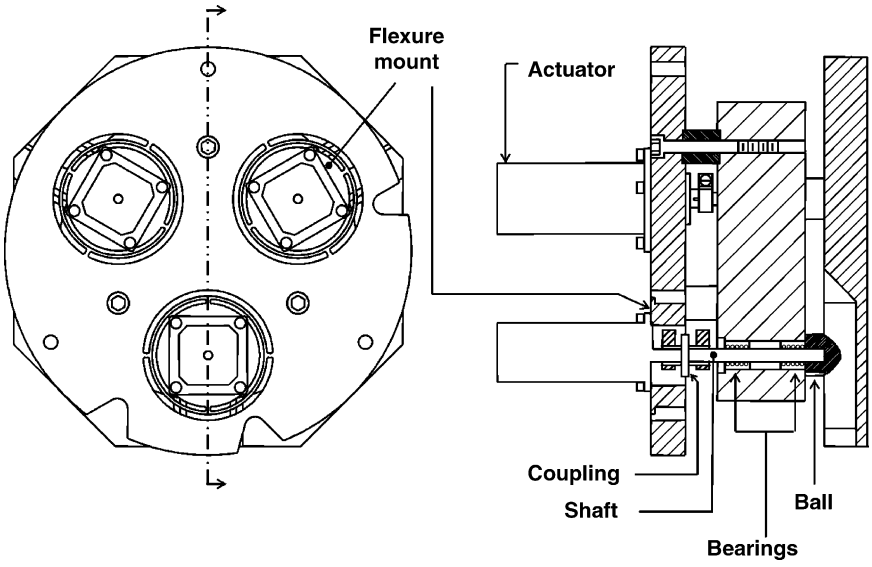

Fig. 16. Detailed cross section of the actuated eccentric ball–shaft fixture.

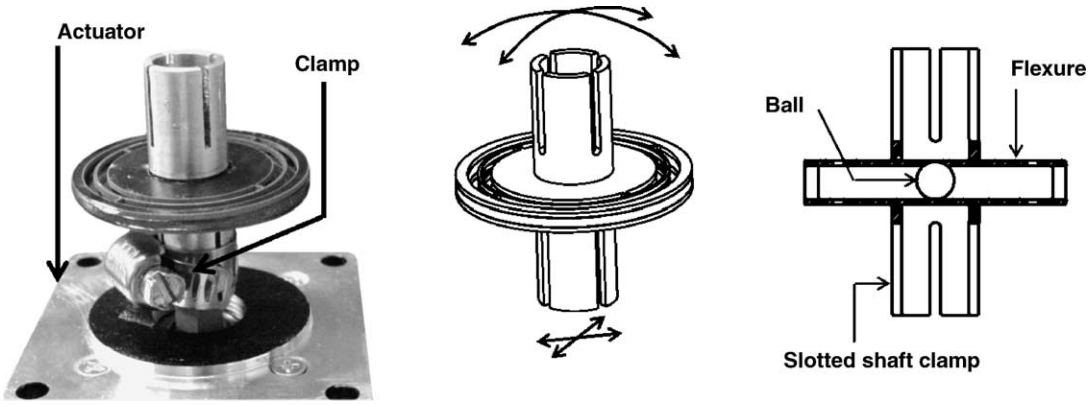

Fig. 17. Actuator–shaft coupling. Left: coupling. Center: flexure degrees of freedom. Right: cross section of coupling.

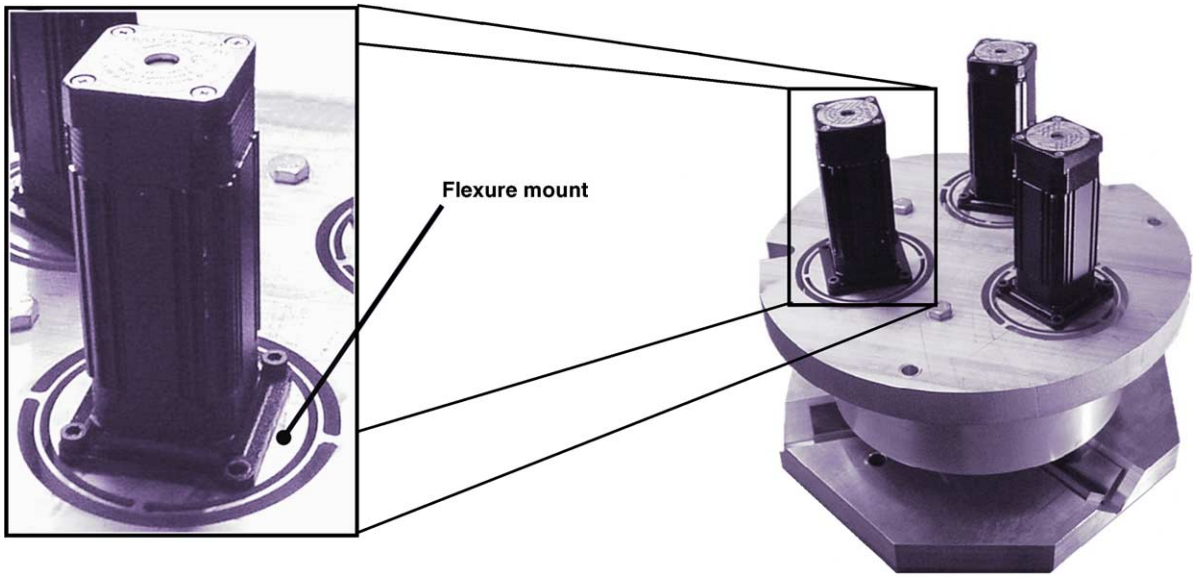

Fig. 18. Four degree-of-freedom actuator flexure mount.

optimization of the four degree-of-freedom coupling with the current packaging constraints.

4.7. Actuator shaft collar

Run out of the actuators was measured at 25 μm. A collar was bonded to the end of each actuator shaft, the actuator was mounted in a mill, run at maximum rotational speed, and then a milling tool was used to true the outer diameter of the collar to better than 5 μm run out. The collar's outer diameter served as the attachment points for the four DOF shaft couplings.

5. Experimental validation of kinematic model

5.1. Experimental setup

Fig. 19 shows the fixture mounted within an automated test rig. This test rig is equipped with an air piston which applies a 550 N nesting preload. A flexure and a wobble pin between the fixture and piston were used to decouple off-axis preload displacements. A DSpace^{TM} control cycles the air piston preload and acquires readings from six capacitance probes. High-pressure grease was used at the ball–groove interface to reduce frictional hysteresis and contact wear. The fixture was calibrated by aligning each ball's eccentricity vector to its groove using a ball bearing as shown in Fig. 20. The notch in the side of the ball is positioned to be symmetric about a plane containing the shaft axis and the center of the ball. The test setup was placed on an air table and allowed to come to thermal equilibrium within an insulated enclosure.

5.2. Experimental procedure

5.2.1. Open-loop displacement tests

Open-loop displacement tests were run to characterize the fixture's ability to provide pure displacement in each axis. This test procedure is not meant to imply that this device is designed for use only as an open-loop device. Rather, we are using these tests to demonstrate the types of errors and

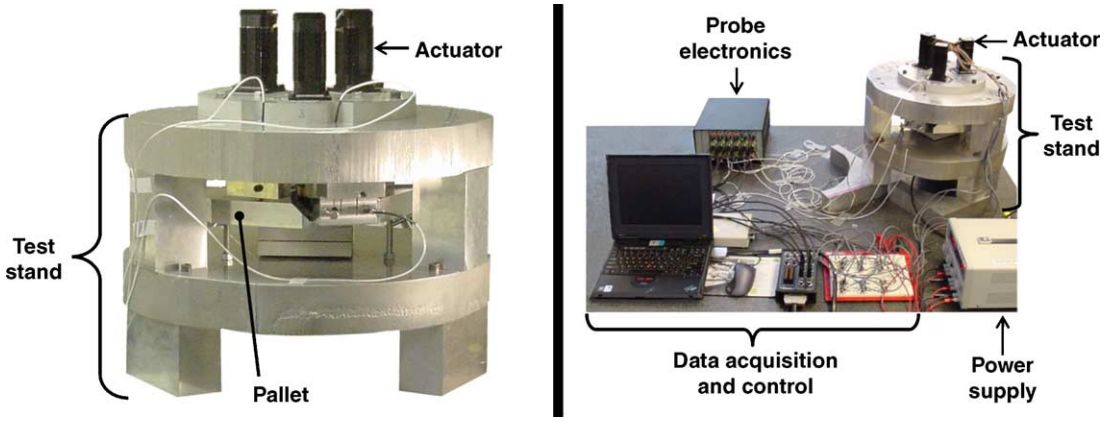

Fig. 19. Experimental setup. Left: coupling mounted in test rig. Right: full experimental setup.

magnitude of errors which precision engineers may expect to address via design improvements, error mapping, compensation, or closed-loop control.

Five positions were measured per test, one at the home position and two on either side of home. Between each position, the preload was removed, the balls were actuated to the desired location and the preload was reapplied. Disengaging while actuating reduces sliding wear at the contact interfaces. The control/data acquisition was programmed to allow the fixture to settle for 30 s once fixtured. Ten readings at each position were taken, and then averaged to obtain the final data point. Each single axis test was completed in less than 2 h. The displacements and parasitic errors measured in each test are provided in Figs. 21 and 22. The data for these plots is provided in the Fig. A.1 within Appendix A. The test setup (capacitance probes, electronics and structure) was capable of resolving displacements of 50 nm. The results in Figs. 21 and 22 will be discussed in Section 6.

5.2.2. Repeatability tests

Two repeatability tests were run to characterize fixture repeatability at the extremes of the mechanism's range; at home and at home + 90°. The control/data acquisition allowed the fixture to settle before each data point was taken. Each test required 17 h to complete. The data obtained for the homed test is provided in Fig. 23. Data obtained from the homed + 90° test (wear-in) is similar in trend to the homed test. We are particularly interested in what can be said about repeatability when the groove and ball surfaces are:

(1) Not yet affected by wear: readings 000–050.
(2) Stabilized (e.g. worn-in): readings 600–900.

The standard deviation of position data for our ranges of interest are tabulated in Table 3.

6. Discussion

6.1. Open-loop displacement tests

A break down of the percent error between predicted and measured data is provided in Table 4. Ninety-six percent of the data is within 10% of predicted values, with one data point as an outlier at 16.4% error. We will revisit the error values

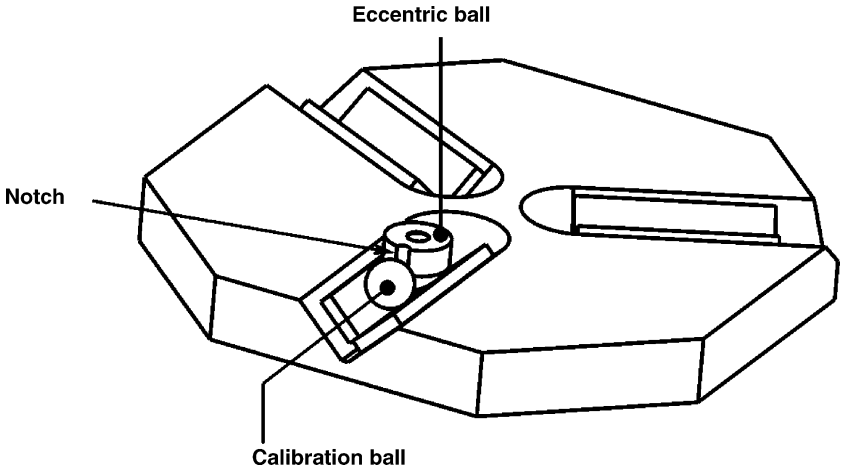

Fig. 20. Use of ball-notch concept to set the in-plane home positions for eccentric balls.

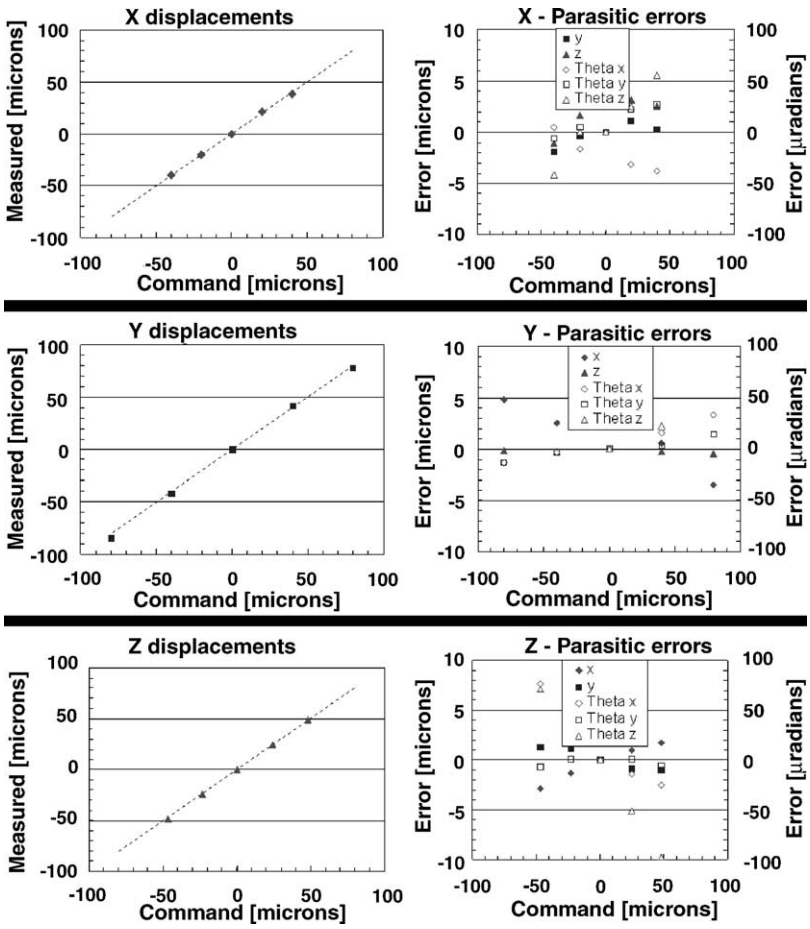

Fig. 21. Left: comparison of commanded linear displacements and measured displacements. Right: parasitic errors for commanded displacements.

after introducing Table 5. The table contains systematic and non-systematic errors expressed as a percent error of the displaced range in each of the six displacement tests. The values were calculated using the scaling laws from Section 3.4 and the average of the homed and home + $\pi/2$ 2σ repeatability for cycles 1–50 (prior to wear-in).

The maximum percent error between theory and measured values is posted in Table 5 in the row titled "maximum theory-measured % error". These values are within the summed error sources for each displacement test with the exception of $\boldsymbol{\theta_z}$ which was out of range by 2.4% error. Additional simulations were run in which it was proven that an additional systematic error of 2% may be attributed to a calibration error associated with the step size, $s_\theta = 0.054^\circ$, of the rotary stepper motors. The important knowledge gained from this exercise is: (1) the need for care in setting the initial orientation of the ball eccentricity vectors and (2) the sensitivity of $\boldsymbol{\theta_z}$ error to rotation step size.

Within the parasitic error plots in Figs. 21 and 22, one can see linear relationships between the commanded displacement and the parasitic errors. These are systematic errors which are proportional to the commanded displacement. The accuracy of the kinematic model, with perfect components, was confirmed to be better than 10 nm/5 μrad (Section 3.3). We are presently investigating second-order geometric imperfections and component compliances which may be

Table 3
Standard deviation of fixture position and orientation

Data range	Fixture position	X (μm)	Y (μm)	Z (μm)	$\boldsymbol{\theta_x}$ (μrad)	$\boldsymbol{\theta_y}$ (μrad)	$\boldsymbol{\theta_z}$ (μrad)
001–050	Homed	0.4	0.8	0.1	2.8	3.3	4.0
	Homed + $\pi/2$	0.7	0.5	0.4	3.8	5.9	2.1
600–900	Homed	1.7	0.7	0.1	1.7	1.9	3.6
	Homed + $\pi/2$	1.4	0.5	0.2	2.2	2.3	1.7
001–900	Homed	1.6	1.1	0.4	3.8	9.9	4.1
	Homed + $\pi/2$	1.4	1.1	0.5	5.4	5.3	2.0

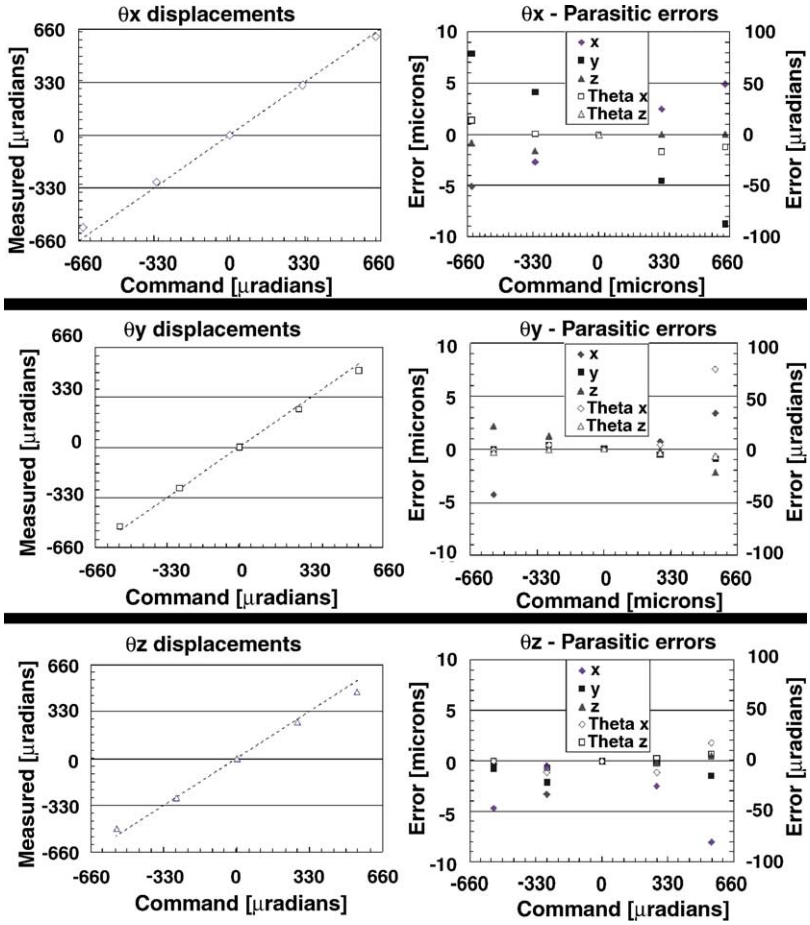

Fig. 22. Left: comparison of commanded rotary displacement and measured displacements. Right: parasitic errors for commanded displacements.

responsible for the errors:

(1) Ball pattern drift due to non-parallelism between the three shaft axes. For instance, if the bearing bores were not machined with perfectly parallel axes, the shafts axes would not be parallel and the in-plane ball patterns would change with out-of-plane actuation.
(2) Ball wobble due to non-parallelism between the axis of symmetry of the balls and their mated shafts.
(3) Bearing compliance errors (Section 6.4) are of the order of 5% of the system compliance.

6.2. Repeatability tests

Results of the repeatability tests were summarized in Table 3. The fresh (001–050 cycles) and worn-in 1σ data (600–900) differ by less than 1.5 μm/2.6 μrad. With this performance, the fixture is suitable for improving the accuracy in several applications. For instance, automotive applications such as sheet metal die alignment, sheet metal-CMM fixturing, engine component manufacturing and part-machine fixturing. The fixture may also find use in semi-conductor test equipment and some optical alignment systems. This experiment has not directly addressed the question of wear-in between many different ball–groove sets. A steady-state wear-in should still occur as the surface asperities within the contact patches (many should overlap) deform and brinell. The coupling accuracy would certainly change as the contacts wear-in, however, the reason for integrating active components is to enable adjustments which correct these types of transient errors.

Table 4
Distribution of percentage error between theory and measurement

Percent error	Percentage of data within this range
0–3	33
3–6	33
6–10	29
10–16	4 (a single data point)

6.3. The potential for improvement in performance

Values for the ratio of IA_{mfg}/IA_{mec} (see Section 3.7) are posted at the bottom of Table 5. The ratios, being larger than unity, indicate that fixture performance may be improved (in some axes more than others) via the use of the mechanism–fixture components.

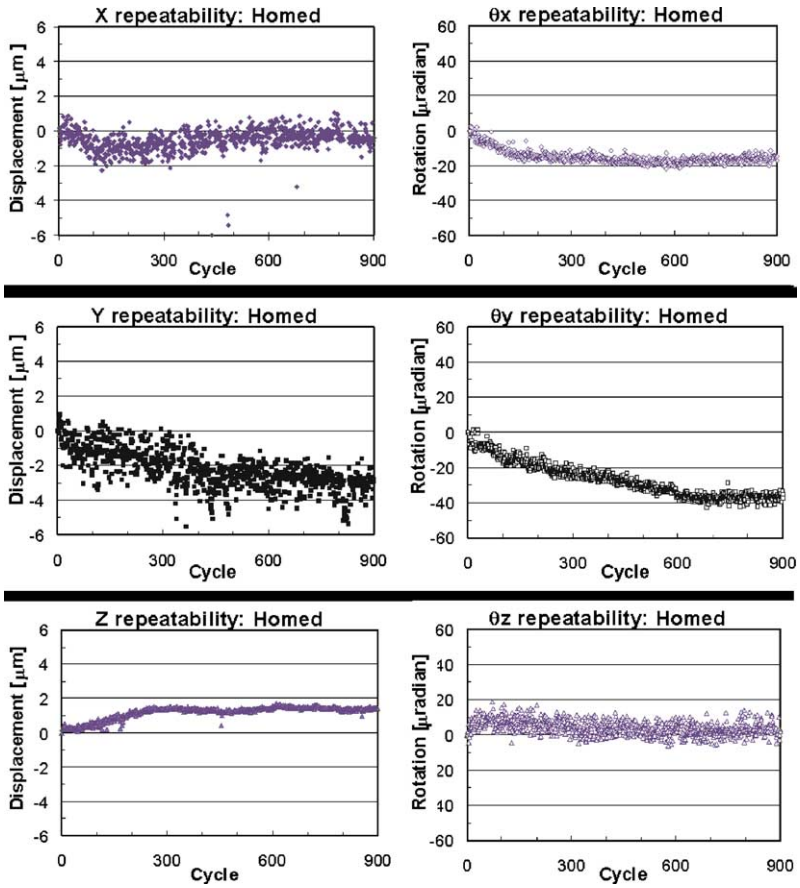

Fig. 23. Centroid displacement as a function of repeated mating cycles.

6.4. *Fixture stiffness*

The integration of bearings into the structural load path will affect the coupling's stiffness. Fig. 24 shows the relationship between coupling preload and the ratio of in-plane bearing stiffness (K_{bip} = 864 N/μm) to in-plane coupling stiffness (K_{cip}) for the prototype under study. The bearing stiffness includes the contributions from six bearings (two per shaft). For a given design, the relationship shown in Fig. 24 enables the designer to select a preload which limits bearing compliance errors to a small amount of the total system compliance error. The preload used in this study, 550 N, yields a stiffness ratio of ∼20.4. The bearing compliance errors should therefore be approximately 5% of the total system compliance. Naturally, higher stiffness bearings and/or ball–groove contacts may be used to reduce the magnitude of compliance errors.

7. Summary and future directions

7.1. *Summary*

We have introduced a mechanism–fixture system design which can be adjusted to provide μm/μrad accuracy

Table 5
2σ Errors as a percentage of displacement range

Type	Error	*X* % error	*Y* % error	*Z* % error	θ_x % error	θ_y % error	θ_z % error
Systematic	Manufacturing tolerance	22.4	11.2	5.6	9.8	12.6	9.4
Non-systematic	Repeatability	1.4	0.8	0.6	0.5	1.0	0.6
	Run out	4.3	8.6	0	0	0	1.8
	Actuation	1.0	0.5	1.2	3.3	4.2	2.2
Total		29.1	21.1	7.4	13.6	17.8	14
Maximum theory-measured % error		6.6	5.7	6.0	9.8	9.4	16.4
IA_{mfg}/IA_{mec}		3.3	1.1	3.1	2.6	2.4	2.0

Average e = 282 μm; R/e = 270; R = 0.076 m; 3σ tolerance = 7 μm; 3σ run out = 1.5 μm; s_θ = 0.054°; s_z = 0.4 μm.

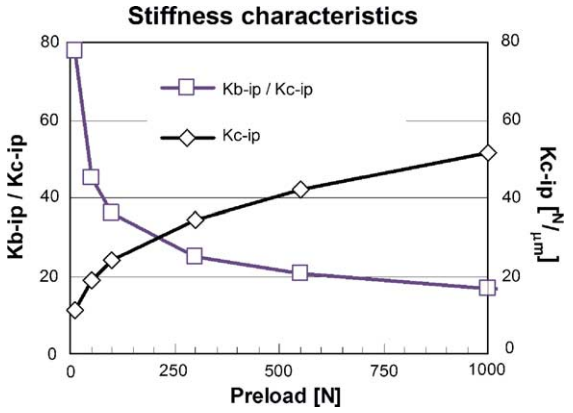

Fig. 24. Relationship between preload and bearing–coupling stiffness ratio.

and repeatability. Kinematic models for a six-axis, eccentric ball–shaft fixture were developed and used to: (1) simulate the effect of tolerances on fixture accuracy and (2) simulate the affect of actuation and bearing run out errors on fixture accuracy. An explanation was provided to demonstrate how to use items 1 and 2 to make cost–performance curves which support design decisions.

7.2. Future applications and directions

Experimental results have been used to validate the kinematic model. The difference between predicted and measured results has been used to identify methods that may improve the performance of the design. The results provide the basis for future work aimed at discovering how to model, design and fabricate mechanism–fixture systems which can provide sub-micron or nanometer-level accuracy and repeatability. Future efforts will be devoted to improving the repeatability of the fixture, modeling parasitic errors and investigating methods used to mitigate fixture wear-in as a source of error in fixture–mechanism systems.

Acknowledgements

This work was supported, in part, by the Ford Motor Company and the Ford–MIT alliance. The authors wish to thank the alliance and Ford Motor Company for their technical and financial support. The authors would also like to thank Mr. Carlos Araque, Mr. Marcos Rodriquez, Mr. Gerry Wentworth and Mr. Mark Belanger for the efforts in fabricating the fixture prototype.

Appendix A

The data obtained from experimental results is tabulated versus theoretical results in Fig. A.1.

x			Parasitic errors					
Theory microns	Experiment microns	Error %	x microns	y microns	z microns	θx μradians	θy μradians	θz μradians
-39.80	-40.00	0.5	---	-1.90	-1.08	4.9	-6.2	-41.8
-20.00	-20.29	1.4	---	-0.34	1.65	-16.6	4.7	0.3
0.00	0.00	0.0	---	0.00	0.00	0.0	0.0	0.0
20.00	21.32	6.6	---	1.10	3.15	-31.2	22.4	25.2
39.80	38.58	-3.1	---	0.24	2.51	-37.5	26.4	55.0

y			Parasitic errors					
Theory microns	Experiment microns	Error %	x microns	y microns	z microns	θx μradians	θy μradians	θz μradians
-80.00	-84.59	-5.4	4.83	---	-0.13	-13.4	-13.4	-265.5
-40.00	-42.44	-5.7	2.51	---	-0.24	-3.5	-3.5	-125.0
0.00	0.00	0.0	0.00	---	0.00	0.0	0.0	0.0
40.00	41.58	-3.8	0.55	---	-0.20	16.1	3.4	22.3
79.78	77.58	2.8	-3.50	---	-0.44	32.9	14.5	110.8

z			Parasitic errors					
Theory microns	Experiment microns	Error %	x microns	y microns	z microns	θx μradians	θy μradians	θz μradians
-46.68	-48.77	-4.3	-2.85	1.29	---	76.2	-6.9	71.5
-22.91	-24.38	-6.0	-1.35	1.11	---	35.4	1.0	35.1
0.00	0.00	0.0	0.00	0.00	---	0.0	0.0	0.0
24.52	24.38	0.6	0.99	-0.89	---	-14.1	0.8	-50.9
48.18	48.77	-1.2	1.67	-1.05	---	-25.5	-5.5	-97.8

θx			Parasitic errors					
Theory microns	Experiment microns	Error %	x microns	y microns	z microns	θx μradians	θy μradians	θz μradians
-640.0	-577.0	-9.8	-5.10	7.88	-0.81	---	13.4	224.3
-320.0	-291.9	-8.8	-2.71	4.10	-1.57	---	0.7	112.7
0.0	0.0	0.0	0.00	0.00	0.00	---	0.0	0.0
320.0	307.8	-3.8	2.46	-4.51	0.07	---	-16.6	-109.6
640.0	611.8	-4.4	4.92	-8.75	0.04	---	-12.5	-209.8

θy			Parasitic errors					
Theory microns	Experiment microns	Error %	x microns	y microns	z microns	θx μradians	θy μradians	θz μradians
-496.5	-471.6	5.3	-4.29	-0.11	2.14	-0.6	---	-3.4
-248.3	-244.6	1.5	-0.09	0.37	1.20	3.8	---	-0.5
0.0	0.0	0.0	0.00	0.00	0.00	0.0	---	0.0
250.0	228.6	9.4	0.67	-0.53	-0.22	4.0	---	-3.8
500.0	462.2	8.2	3.34	-0.89	-2.20	75.5	---	-7.2

θz			Parasitic errors					
Theory microns	Experiment microns	Error %	x microns	y microns	z microns	θx μradians	θy μradians	θz μradians
-492.0	-449.0	9.6	-4.66	-0.72	0.00	0.0	0.0	---
-248.3	-252.6	-1.7	-3.25	-2.07	-0.40	-11.3	-7.0	---
0.0	0.0	0.0	0.00	0.00	0.00	0.0	0.0	---
249.3	232.4	7.3	-2.50	-0.18	-0.16	-11.9	3.1	---
496.9	426.9	16.4	-8.04	-1.43	0.52	17.7	6.8	---

Fig. A.1. Coupling displacement measurements for Figs. 21 and 22.

References

[1] Blanding DL. Exact constraint machine design using kinematic principles. New York: ASME Press; 1999.
[2] Hale LC, Slocum AH. Optimal design techniques for kinematic couplings. Precision Eng 2001;25(2):114–27.
[3] Schouten CH, Rosielle PCJN, Schellekens PHJ. Design of a kinematic coupling for precision applications. Precision Eng 1997;20(1):46–52.
[4] Slocum AH. Design of three-groove kinematic couplings. Precision Eng 1992;14(2):67–73.
[5] Slocum AH. Kinematic couplings for precision fixturing. Part I. Formulation of design parameters. Precision Eng 1988;10(2):85–91.
[6] Slocum AH, Donmez A. Kinematic couplings for precision fixturing. Part 2. Experimental determination of repeatability and stiffness. Precision Eng 1988;10(2):115–22.
[7] Barraja M, Vallance RR. Tolerance allocation for kinematic couplings. In: Proceedings of the 2002 Summer Topical Meeting of the American Society for Precision Engineering, Charlotte, NC; July 2002.
[8] Culpepper ML. Design of quasi-kinematic couplings. Precision Eng 2004;28(3):338–57.
[9] Culpepper ML, Slocum AH, Shaikh FZ, Vrsek G. Quasi-kinematic couplings for low-cost precision alignment of high-volume assemblies. J Mech Des 2004;126(4):456–63.
[10] Taylor JB, Tu JF. Precision *X–Y* microstage with manoeuvrable kinematic coupling mechanism. Precision Eng 1996;18(2):85–94.

[11] Conversations with Eugene Gleason of Bal-tech with regard to three axis adjustable kinematic mounts; December 2001.
[12] Culpepper ML, Araque C, Rodriquez M. Design of accurate and repeatable kinematic couplings. In: Proceedings of 2002 Annual Meeting of the American Society for Precision Engineering, St. Louis, MO; October 2002. p. 279–84.
[13] Culpepper ML, Slocum AH, DiBiasio CM. Design of detachable precision fixtures which utilize hard and lubricant coatings to mitigate wear and reduce friction hysteresis. In: Proceedings of the 2003 Annual Meeting of the American Society for Precision Engineering, Portland, OR; October 2003.